Sound Propagation around Underwater Seamounts

by

Joseph J. Sikora III

Submitted to the Department of Electrical Engineering and Computer Science in partial fulfillment of the requirements for the degree of

Master of Science

at the

MASSACHUSETTS INSTITUTE OF TECHNOLOGY

and the

WOODS HOLE OCEANOGRAPHIC INSTITUTION

August 2005

Signature of Author .....
Department of Electrical Engineering and Computer Science
August 8, 2005

Certified by .....
Arthur B. Baggeroer, Thesis Supervisor
Ford Professor of Engineering
Secretary of the Navy/Chief of Naval Operations Chair for Ocean Sciences
Massachusetts Institute of Technology

Accepted by .....
Mark Grosenbaugh
Chair, Joint Committee in Applied Ocean Science and Engineering,
MIT/WHOI

Sound Propagation around Underwater Seamounts

by

Joseph J. Sikora III

Submitted to the Department of Electrical Engineering and Computer Science
on August 8, 2005, in partial fulfillment of the
requirements for the degree of
Master of Science in Electrical Engineering and Computer Science

Abstract

This thesis develops and utilizes a method for analyzing data from the North Pacific Acoustic Laboratory's (NPAL) Basin Acoustic Seamount Scattering Experiment (BASSEX). BASSEX was designed to provide data to support the development of analytical techniques and methods which improve the understanding of sound propagation around underwater seamounts.

The depth-dependent sound velocity profile of typical ocean waveguides force sound to travel in convergence zones about a minimum sound speed depth. This ducted nature of the ocean makes modeling the acoustic field around seamounts particularly challenging, compared to an isovelocity medium. The conical shape of seamounts also adds to the complexity of the scatter field. It is important to the U.S. Navy to understand how sound is diffracted around this type of topographic feature. Underwater seamounts can be used to conceal submarines by absorbing and scattering the sound they emit.

BASSEX measurements have characterized the size and shape of the forward scatter field around the Kermit-Roosevelt Seamount in the Pacific Ocean. Kermit-Roosevelt is a large, conical seamount which shoals close to the minimum sound speed depth, making it ideal for study. Acoustic sources, including M-sequence and linear frequency-modulated sources, were stationed around the seamount at megameter ranges. A hydrophone array was towed around the seamount to locations which allowed measurement of the perturbation zone.

Results from the method developed in this thesis show that the size and shape of the perturbation zone measured coincides with theoretical and experimental results derived in previous work.

Thesis Supervisor: Arthur B. Baggeroer
Title: Ford Professor of Engineering
Secretary of the Navy/Chief of Naval Operations Chair for Ocean Sciences

Acknowledgments

I wish to thank Dr. Arthur Baggeroer for supporting my research and education at both the Massachusetts Institute and Technology and the Woods Hole Oceanographic Institute. Both institutions have been wonderful places to conduct research, to interact with world-class engineers and scientists, and to meet many new friends. The opportunities to participate in research cruises and conferences have contributed significantly to my understanding of ocean acoustics and signal processing.

BASSEX, the source of data for my research, was ably planned and executed by Dr. Baggeroer, Keith von der Heydt of WHOI, and Dr. Kevin Heaney of OASIS Incorporated.

Kevin Heaney enhanced my general understanding of underwater acoustics and the purpose of the NPAL experiments, during free moments on the NPAL cruise and at Acoustical Society of America conference in Vancouver.

Kyle Becker, and the team from Pennsylvania State University, did an excellent job operating the towed hydrophone array used during the BASSEX experiment.

Thanks also to Edward Sheer for patiently guiding me through some knotty problems I had with my beamformer and matched filtering, and to Dr. William Siegmann, who provided me with an undergraduate research project developing poro-elastic wave speed equations, which has led to my current work at MIT and WHOI.

Lastly, I would like to thank my father, Joseph J. Sikora II, who has helped me throughout my undergraduate and graduate education. The knowledge and experience gained from his education and career as an electrical engineer have been an invaluable asset.

Contents

List of Figures

List of Tables

Chapter 1

Introduction

This thesis describes my research on long-range underwater sound propagation around seamounts using data from the NPAL 2004 BASSEX experiment.

Understanding how sound propagates through range-dependent ocean waveguides is a particularly challenging field due to the complexity and scale of the environment.

1.1 Motivation

My research was supported by the United States Navy, Office of Naval Research, contract number N00014-04-1-0124. The general goal my research is to improve the understanding of underwater acoustics.

The primary application of my work is to improve our ability to detect and conceal submarines, particularly behind seamounts. Seamounts are a common topographic feature in many of the world's oceans. Underwater seamounts can be used to hide submarines by absorbing and reflecting the sound they emit.

Another possible application is to aid in the detection of illegal underwater nuclear weapons testing as part of the Comprehensive Test Ban Treaty Organization.

The depth-dependent sound velocity profile of typical ocean waveguides force sound to travel in convergence zones about a minimum sound speed depth. This ducted nature of the ocean, the so called SOFAR channel [1], makes modeling the

acoustic field around seamounts particularly challenging, compared to an isovelocity medium. The conical shape of seamounts also adds to the complexity of the scatter field.

This research will be used to better understand how seamounts affect low-frequency sound wave propagation to help detect and conceal submarines.

1.2 Previous Work

Acoustic field scattering by seamounts has been examined through experimentation and acoustic theory. However, due to the complexity of the problem, results found in the literature fail to provide a complete understanding of how seamounts scatter acoustic energy.

1.2.1 Experimental approach to the problem

Wage [2] analyzed data taken from the Acoustic Thermometry of Ocean Climate (ATOC) experiment, where a source, moored on the Pioneer Seamount, transmitted a signal to vertical line arrays in Hawaii and Kiritimati. She showed that the Pioneer Seamount was responsible for weak, late arrival signals in the receptions, and that modes 1 through 10 have low coherence at megameter ranges. The effects that seamounts have on sound propagation is therefore of interest, and a complete understanding of these effects is important to the field of underwater acoustics.

Ebbeson and Turner [3] used experimental results and ray tracing to measure the scattering field around the Dickins Seamount in the Northeast Pacific Ocean. They showed that the acoustic energy inside the shadow zone can drop as much at 15dB, compared with that of the field outside the shadow zone, and that the shape of the shadow zone corresponds roughly to the projected width of the seamount.

1.2.2 Theoretical approach to the problem

Taroukadis [4] modeled a seamount as a set of superimposed rings, where each of the rings is a range-independent environment. This method, however, can yield numerically unstable results. Inspired by Taroukadis, Eskenazi [5] modeled a seamount with cylinders, of decreasing diameter, stacked on top of one another. He used a Direct Global Matrix approach for numerically modeling the size of the perturbation zone around a seamount, for a point source, which offered better numerical stability. The results from his work show that a perturbation zone appears behind seamounts and fans out with boundaries on each side tangent to the seamount and passing through the source. The perturbation zone can contain regions of higher or lower acoustic energy than the region outside of the zone the same distance away from the source. He also showed that the perturbation zone "heals" itself a far enough distance away from the seamount.

1.3 Experimental Approach

Eskenazi's work provides, in part, the background for my research. He suggested the necessity of experimental verification of his numerical simulations, in particular the shape of the perturbation zone behind a seamount.

One of the goals of the BASSEX experiment was to measure this perturbation zone around the Kermit-Roosevelt Seamount in the Pacific Ocean using a towed hydrophone array and broadband point sources in the 0-250Hz range. My work involved gathering and analyzing data from the hydrophone array recorded near the Kermit-Roosevelt Seamount when the point sources were active. To accurately verify theoretical results, multibeam echo depth sounding was performed to measure the complex bathymetry around the seamount and expendable bathythermometers were launched to measure sound velocity profiles. The Kermit-Roosevelt Seamount was expected to scatter energy in a manner consistent with the cylindrical seamount model explored by Eskenazi; however, the size and shape of the two types of seamounts are

not the same.

From previous experiments, theoretical results, and Huygen's principle, I assert that seamounts should block sound propagation in such a way that a fan shaped shadow zone appears behind them containing regions of high and low signal energy relative to the surrounding area.

1.4 Roadmap

This thesis is organized in the following fashion:

Chapter 2 - Background, describes environment and equipment used in the experiments

Chapter 3 - Data Analysis, describes beamforming techniques and matched filtering

Chapter 4 - Results, describes and discusses results

Chapter 5 - Conclusion, summarizes the results and offers suggestions for future work

Appendix A - contains nomenclature used in beamformer and matched filter development

Appendix B - contains computer hardware and software information

Appendix C - figures showing processed data and charts from Day 264

Appendix D - figures showing processed data and charts from Day 265

Appendix E - figures showing processed data and charts from Day 267

Appendix F - figures showing processed data and charts from Day 268

Chapter 2

Background

A simplified view of seamounts is to treat them as cylindrical objects in the ocean. A plane wave propagating through the ocean would be blocked by the seamount, but propagate undisturbed everywhere else. Christian Huygens (1629-1695), the Dutch physicist-astronomer, hypothesized that every point on an advancing wavefront can be treated as an spherically spreading point source in an isotropic medium [6]. This implies that the wavefronts not blocked by the seamount would act as two continuous line arrays starting at the seamount and extending to plus and minus infinity.

In the far-field, or beyond the Fresnel distance [7], the perturbation in the acoustic field from the seamount will be small compared with that of the original plane wave. This could be referred to as the healing distance of the perturbation zone, where the field has approximately the same amplitude and phase as would exist if no seamount were present in the waveguide.

It is with this principle, previous work, and U.S. Navy concerns that an experiment was designed to measure the scattering field around a seamount.

2.1 The BASSEX/SPICEX/LOAPEX Experiments

NPAL is an experiment, funded by the Office of Naval Research (ONR), to test the limits of underwater acoustics and improve our understanding of the ocean. One of

the goals of NPAL is to better understand how ocean variability and the ambient sound field affect long-range acoustic propagation [8].

After the Acoustic Thermometry of Ocean Climate (ATOC) demonstration, ONR began sponsorship of NPAL; ATOC showed that a small number of acoustic transmitters and receivers could adequately characterize temperature changes across an entire ocean basin. In 2004, NPAL was funded to conduct the SPICEX, LOAPEX, and BASSEX experiments. All three experiments were coincident upon each other and ran between September and October of 2004.

Three acoustic transceivers were moored prior to the experiments, two south of the Kermit-Roosevelt Seamount Complex in the central Pacific Ocean and one offshore of Kauai Island, Hawaii. Two automated vertical line arrays (VLA's) were also moored before the experiments. The VLA's were designed to listen to the moored sources and to ship-deployed sources. Tables 2.1 through 2.3 describe each of the sources used during the experiments [8].

Two ships were used during the experiments, the *R/V Roger Revelle* and the *R/V Melville*. The *R/V Melville* carried an acoustic transceiver, deployed using the ship's A-frame. The transceiver was lowered into the water at various stations across the Pacific Ocean and transmitted M-sequences and prescription frequency modulated (PFM) signals. The *R/V Roger Revelle* towed the Five Octave Research Array, a horizontal hydrophone array designed to listen to all of the sources deployed during these experiments.

2.1.1 SPICEX

The SPICEX experiment was designed to measure ocean "spiciness," a term referring to salinity, temperature, and pressure variations that mimic ocean internal waves. (Wage's [2] work, discussed earlier, showed how Garret-Munk internal waves reduced modal coherence at megameter ranges.) These variations add randomness to the sound velocity profile of the ocean, altering sound paths. SPICEX measured ocean spiciness between the moored sources and VLA's. Figure 2-1 is an example temper-

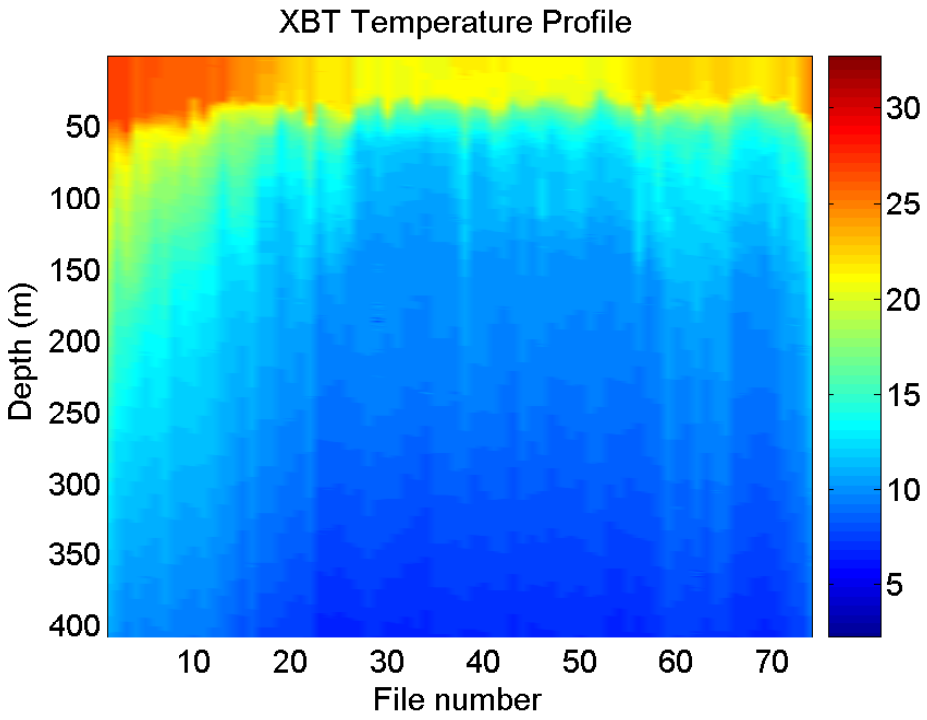

Figure 2-1: SPICEX Temperature Data (°C)

ature profile taken during the NPAL experiment to help understand ocean spiciness. Figure 2-2 is a chart containing the locations of the VLA's and the moored sources during the experiments.

2.1.2 LOAPEX

The Long-range Ocean Acoustic Propagation Experiment, or LOAPEX, was designed to study the evolution of the acoustic arrival pattern with range, understand acoustic energy transmission below critical depth, and observe the effects of bottom interaction on sound propagation. The experiment used the source deployed by the *R/V Melville*, which moved to each station, shown in figure 2-2, and transmitted M-sequence and PFM signals. VLA's deployed for the SPICEX experiment were also used during the LOAPEX experiment to listen to the signals arriving from the *R/V Melville* and to the source off-shore of Kauai Island.

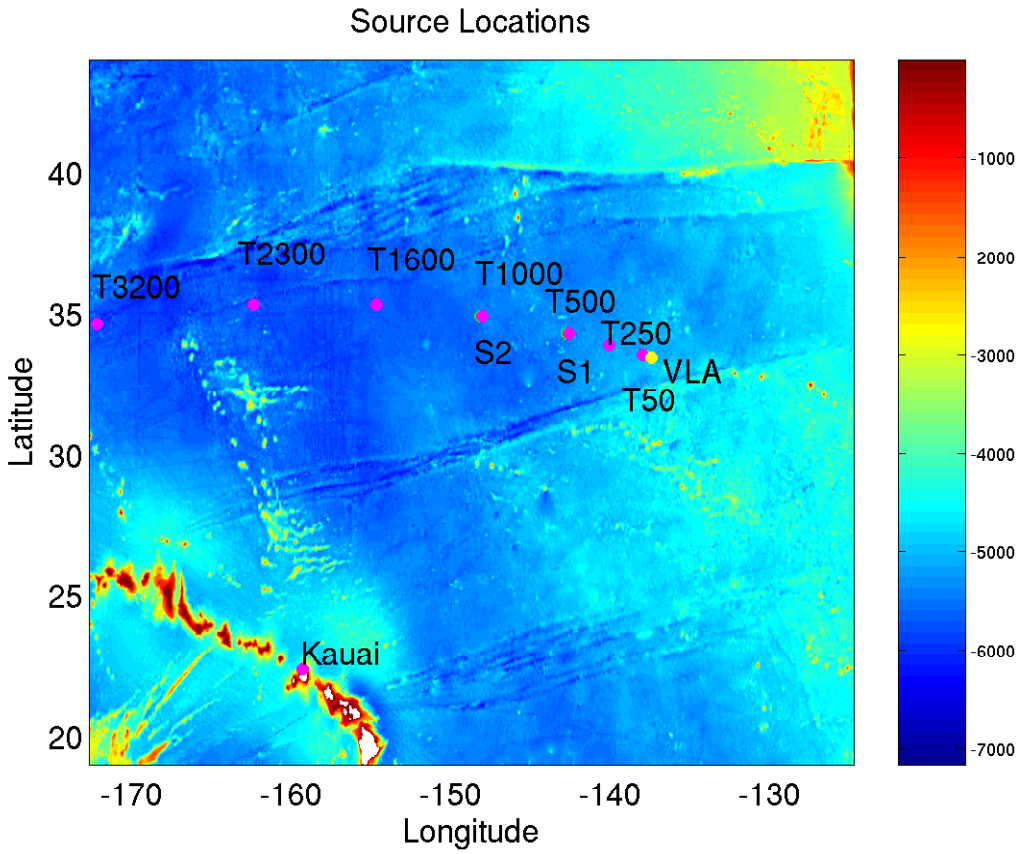

Figure 2-2: Source Positions: (S) SPICEX moored source, (T) LOAPEX stations

Table 2.1: Kauai Source

ATOC/NPAL Kauai Source		
center frequency	75	Hz
cycles/digit	2	
digit length	26.6667	msec
sequence length	1023	digits (degree 10)
sequence period	27.2800	sec
sequence law	3471_8	
artifact location	474	
sequence initialization	1000_8	
phase modulation angle	89.209215°	
sequence repetitions transmitted	44	
transmission duration	1200.3200	sec
source level	195	dB re 1 μPa at 1 m
latitude	22°20.949360’	N
longitude	159°34.195440’	W
depth	811	meters
distance to Kermit-Roosevelt Seamount	2,253	km

Table 2.2: LOAPEX Sources

center frequency	68	75	Hz
law [octal]	2033	2033	
cycles/digit	2	2	
sequence period	30.0882	27.2800	sec
digits	1023	1023	
phase modulation angle	89.209215°	89.209215°	
source level	194-195	195	dB re 1 μPa at 1 m
depth	350-500	800	meters

Transponder	Latitude N	Longitude W	Depth (m)
T50	33°30.1739'N	138°09.1720'W	5176
T250	33°51.7400'N	140°16.7100'W	
T500	34°14.4812'N	142°49.7375'W	5366
T1000	34°51.4010'N	148°13.5529'W	5286
T1600	35°17.0151'N	154°53.7680'W	
T2300	35°18.8621'N	162°34.9580'W	5868
T3200	34°38.3490'N	172°24.4210'W	

Table 2.3: SPICEX Sources

HLF-5 Acoustic Sources		
center frequency	250	Hz
cycles/digit	2	
digit length	12.0000	msec
sequence length	1023	digits (degree 10)
sequence period	12.2760	sec
sequence initialization	1000_8	
phase modulation angle	89.209215°	
sequence repetitions transmitted	11	
transmission duration	135.0360	sec
source level	192	dB re 1 μPa at 1 m
distance to Kermit-Roosevelt Seamount (S1)	616.8	km
distance to Kermit-Roosevelt Seamount (S2)	503.9	km

Source	Sequence Law	Artifact Location	Latitude	Longitude	Depth
S1	2033_8	531	34°19.46'N	142°58.82'W	750 m
S2	3471_8	474	34°58.49'N	148°22.68'W	750 m

2.1.3 BASSEX

The Basin Acoustic Seamount Scattering Experiment (BASSEX) was designed to measure the scattering effects of the Kermit-Roosevelt Seamount and characterize bottom interaction around the Kauai source.

Sound/sea floor interaction

The Kauai source is a 75Hz M-sequence source located 811 meters below the surface of the ocean. The gradually down-sloping ocean bottom makes off-shore Kauai Island an ideal location for measuring sound/sea floor interaction.

Seamount scattering

The Kermit-Roosevelt Seamount is one of the largest seamounts in the world. It shoals at roughly 900 meters in a region of the ocean with an average sea floor depth of approximately 5000 meters. Just to the south-east of the Kermit Seamount is a smaller seamount (nicknamed "Elvis") that shoals at 1300 meters. The size of these seamounts make them ideal to measure the scattering field of a seamount.

2.2 The BASSEX Experiment

On September 13th, 2004, along with my advisor, I joined the scientific crew aboard the *R/V Roger Revelle* in Honolulu, Hawaii. Our primary mission was to tow the ONR Five Octave Research Array around the Kermit-Roosevelt Seamount Complex, around the SPICEX sources, and off-shore Kauai Island. Onboard the research vessel I recorded array data, processed multibeam echo sounder data, and launched expendable bathythermometers (XBT's).

To measure the length of the perturbation zone behind the seamount, the array was towed along paths that intersected the seamounts and the desired sources. The array was also towed perpendicular to these paths in order to obtain a measurement

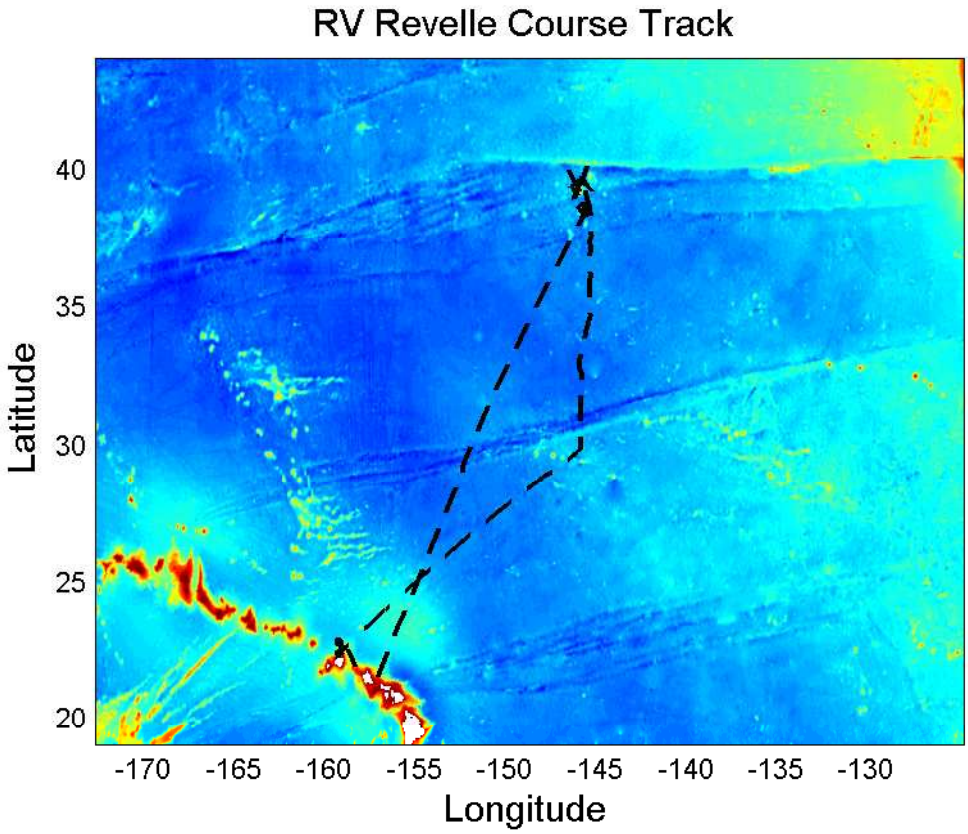

Figure 2-3: Ship course during NPAL experiment

of the width of the perturbation zone behind the seamount. Back scattering was measured by towing the array in front of the seamounts, relative to the source. Forward scattering was measured by towing the array behind and directly over the seamounts, relative to the source. Figure 2-3 shows the ship track of the *R/V Roger Revelle* throughout the experiment.

2.2.1 Multibeam Bathymetry

During the seamount scattering part of the BASSEX experiment, multibeam bathymetry data was recorded to obtain an accurate measure of the size and shape of the seamounts. This was important because of inconsistencies we discovered, prior to the experiment, between available bathymetry databases, including the Smith-Sandwell bathymetry database [9], version 8.2, and the General Bathymetry Chart of the Ocean (GEBCO) [10]. These databases do provide a consistent location for the seamounts,

which allowed us to plan the course of the *R/V Roger Revelle* before the experiments got underway.

The EM120 Multibeam Swathbathymetry Echo Sounder operated at 12kHz and used 191 beams covering up to 150 degrees to get high resolution bathymetry while underway. Figures 2-4 and 2-5 show the multibeam bathymetry gathered around the Kermit-Roosevelt Seamount Complex with a cubic interpolation applied to fill in regions where data was not available.

2.2.2 Expendable Bathythermometers (XBT's)

XBT's are designed to measure temperature versus depth in the ocean. An XBT was launched every four hours during the cruise. This data, as well as salinity, were used to determine ocean spiciness and the sound velocity profile of the ocean. The relationship between temperature, depth, salinity and sound speed is given by [11]

$$\begin{aligned} c = 1449.2 + 4.6T - 0.055T^2 + 0.00029T^3 \\ +(1.34 - 0.01T)(S - 35) + 0.016z. \end{aligned} \tag{2.1}$$

Sippican T-5 XBT's, capable of ± 0.1°C and 65 cm accuracy, were used throughout most of the cruise to gather temperature data. Figure 2-6 shows an example temperature file from a typical XBT cast and figure 2-7 shows the sound velocity profile derived from the temperature profile using available salinity data.

2.2.3 Five Octave Research Array

The Five Octave Research Array, or FORA, is a towed 162 element nested hydrophone array developed by Pennsylvania State University and the Chesapeake Science Corporation. The acoustic sensors on the array are non-linearly spaced, designed to maintain a relatively constant main lobe width for broadband beamforming. The array is designed to listen to sound at frequencies around 250Hz (3 meter spacing in 1500m/s water) without aliasing; see Van Trees [12]. The sampling rate of the array

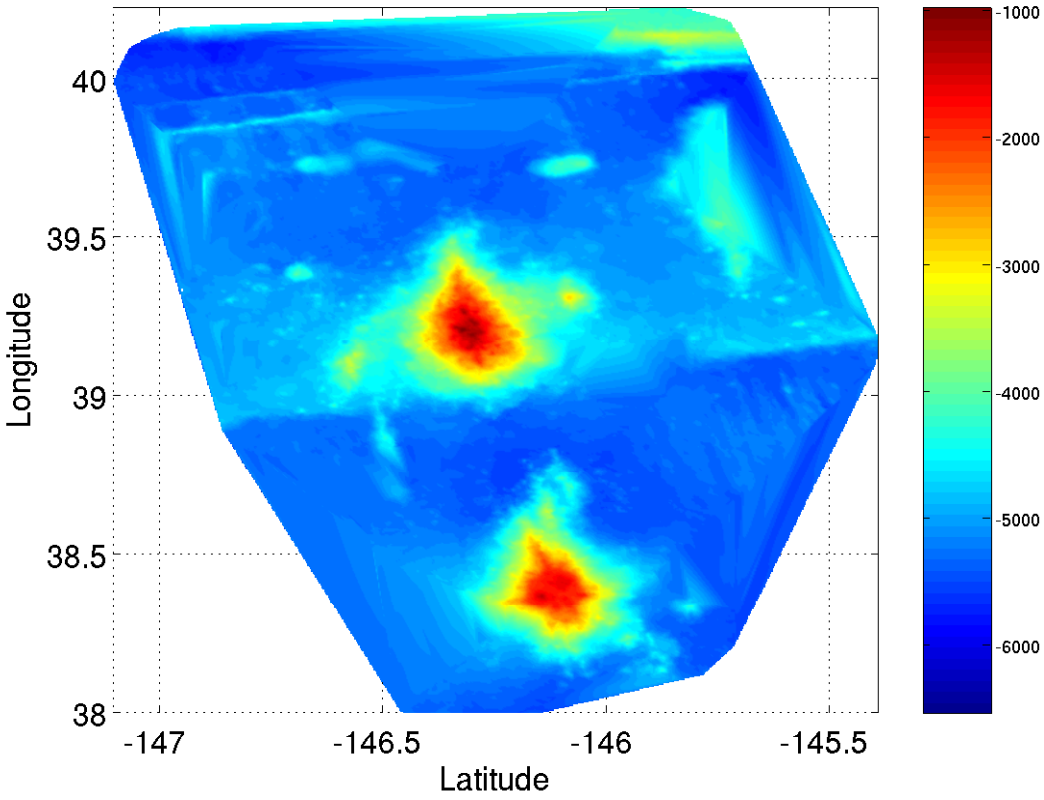

Figure 2-4: Multibeam bathymetry: top-down view

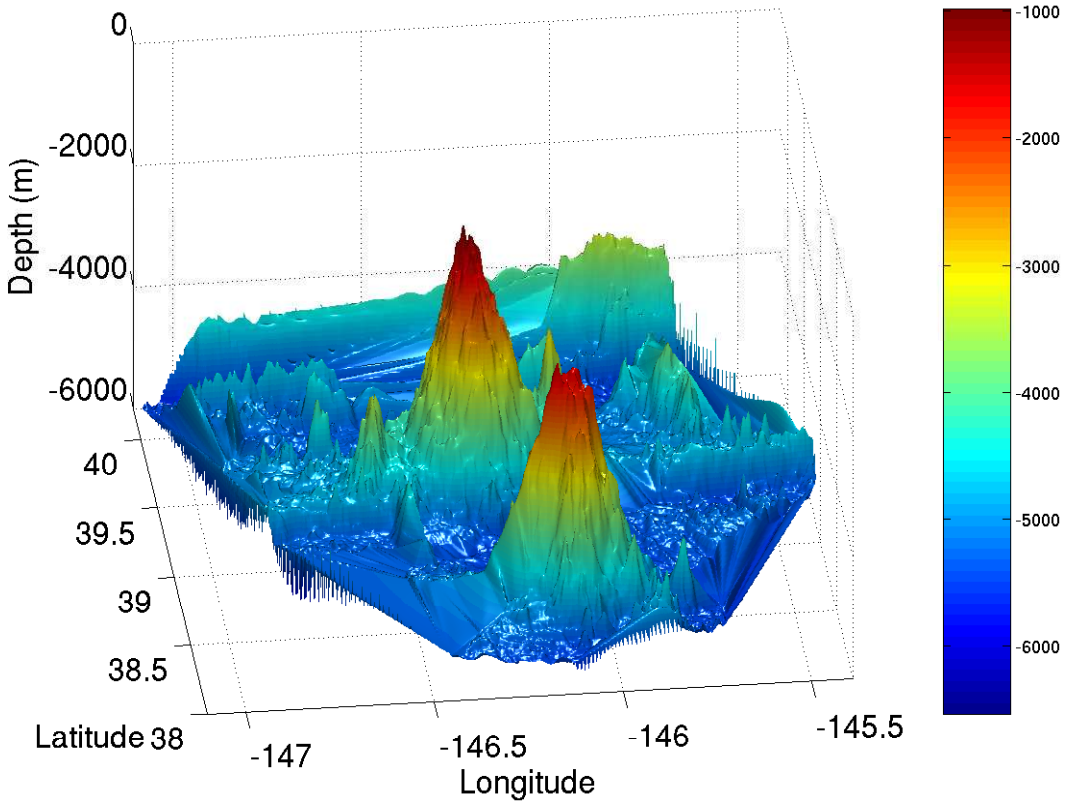

Figure 2-5: Multibeam bathymetry: isometric view

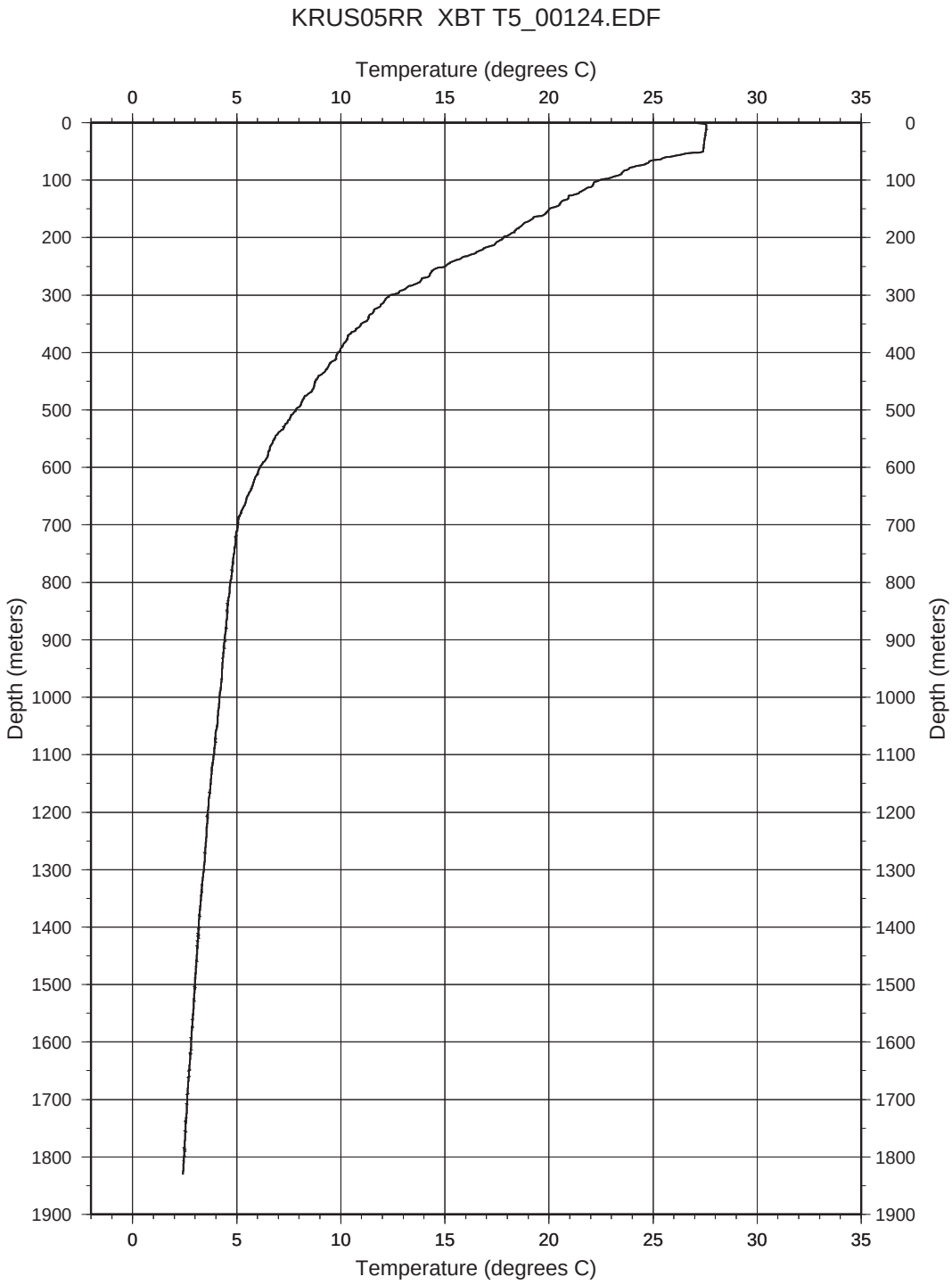

Figure 2-6: XBT example: temperature profile

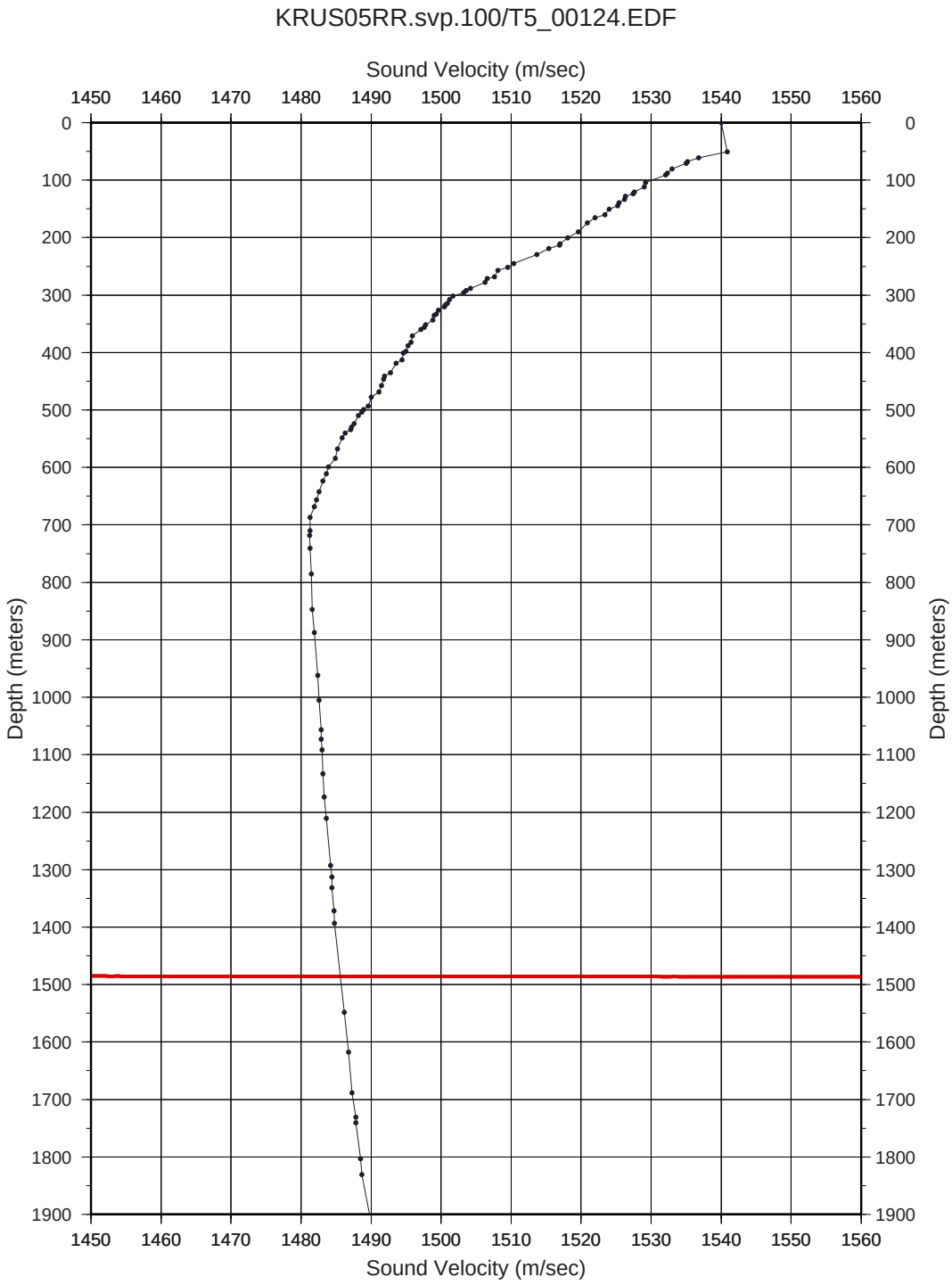

Figure 2-7: XBT example: sound velocity profile

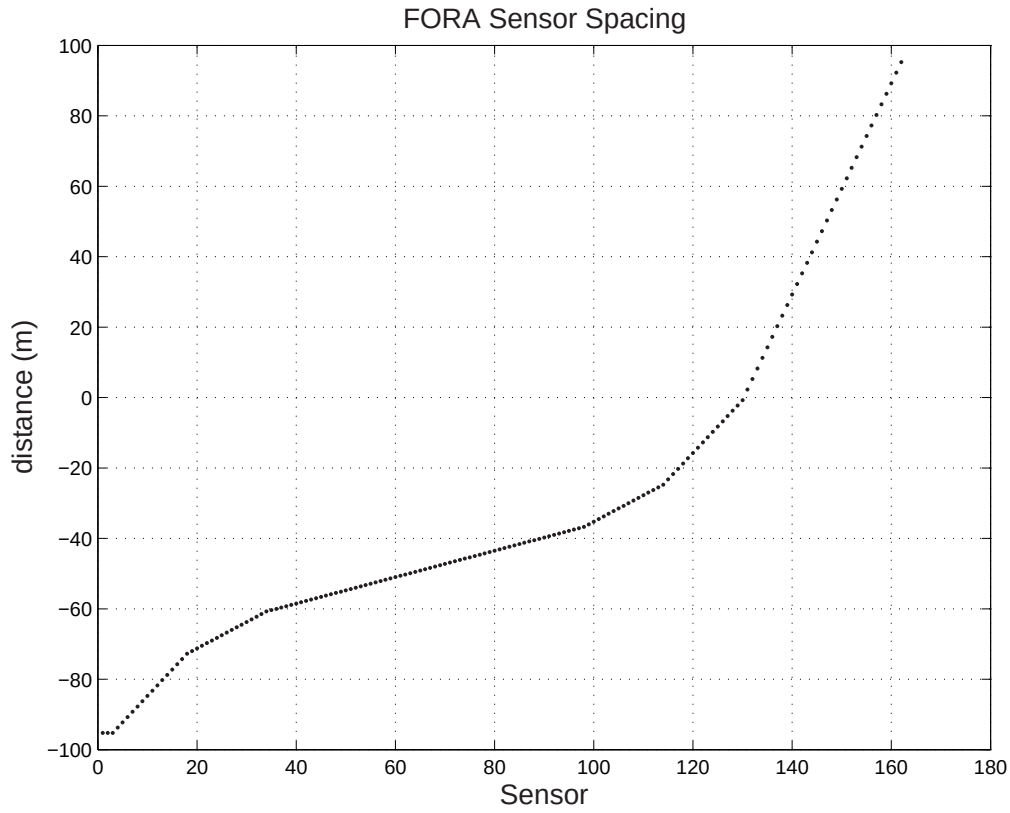

Figure 2-8: Five Octave Research Array Sensor Spacing

is 6250Hz. The array was towed at approximately 3-4 knots at a depth of about 300 meters throughout the experiment. The array was operated by a team from Pennsylvania State University, led by Kyle Becker. Figure 2-8 shows the array sensor spacing.

2.3 Summary

All of the NPAL experiments were generally very successful. Throughout the experiments the *R/V Roger Revelle* crew made 316 recordings, containing 738 transmissions, with the FORA array. The data files were large due to the high, 6250Hz sampling frequency of the array, and were thus decimated to a 781.25Hz sampling rate.

In the following chapters, I will lay out the process through which I calculated

the acoustic energy from the BASSEX array recordings to determine the size and shape of the perturbation zone around the Kermit-Roosevelt Seamount. Only data files containing transmissions from the two SPICEX sources were processed. Results will be compared with previous work.

Chapter 3

Data Analysis

The goal of my research was to measure the size and shape of the acoustic perturbation zone created behind seamounts in the ocean. Adaptive beamforming and matched filtering were used to calculate the amount of acoustic energy measured for each M-sequence reception recorded during the cruise. The location of each reception was determined using Global Positioning coordinates; error in WAAS enabled GPS is often less than 5m and has little effect on my results because of the relative scale of the perturbation zone [13].

3.1 Beamforming

Beamforming is a process by which the outputs of an array are weighted by gains and time shifts in order to filter signals in a space-time field [12]. There are many applications for beamforming, including array steering and reducing signal interference.

3.1.1 Array Steering

During the experiment it was common for two signals to arrive at the same time. The course of the ship was charted in such a way that the direction of arrival for each of the overlapping signals was always different. This allowed us to electronically "steer" the array in the direction of one signal and filter out the other.

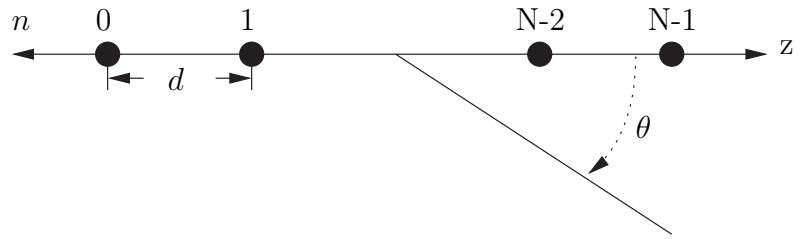

Figure 3-1: Linear array along z-axis

Figure 3-1 shows a linear array which is a crude model for the FORA towed array used in our experiment. The symbol θ represents the arrival angle of a plane wave signal incident on the array. An angle of 0° is referred to as endfire and angle of 90° is referred to as broadside. The black dots in the figure represent the N hydrophones in the array, where d is the spacing between them.

Time delays are applied to each sensor output to steer an array. The steering direction will be referred to as θ_s. The time delay of each sensor must be the same as the travel time of a plane wave, arriving at θ_s, from a reference sensor. The time delay to be applied to sensor n is

$$\tau_n = \frac{p_n \cos\theta_s}{c}, \tag{3.1}$$

where p_n is the distance from the reference sensor and c is the speed of the plane wave. For a horizontal towed array, plane waves arriving at any angle about the axis of the array will have the same sensor arrival times. This results in port/starbord ambiguity; an important property to account for when planning the NPAL experiments.

Figure 3-2 shows the beampatterns for a linear, uniformly spaced line array with arbitrary values for frequency, sound speed, sensor number and spacing chosen. The beampatterns give arrival direction versus attenuation, a measure of a beamformer's ability to remove unwanted signals. The broadside beamformer clearly has a better resolution than the endfire beamformer. This characteristic makes it important to keep the array physically positioned so desired signals arrive close to broadside, whenever possible.

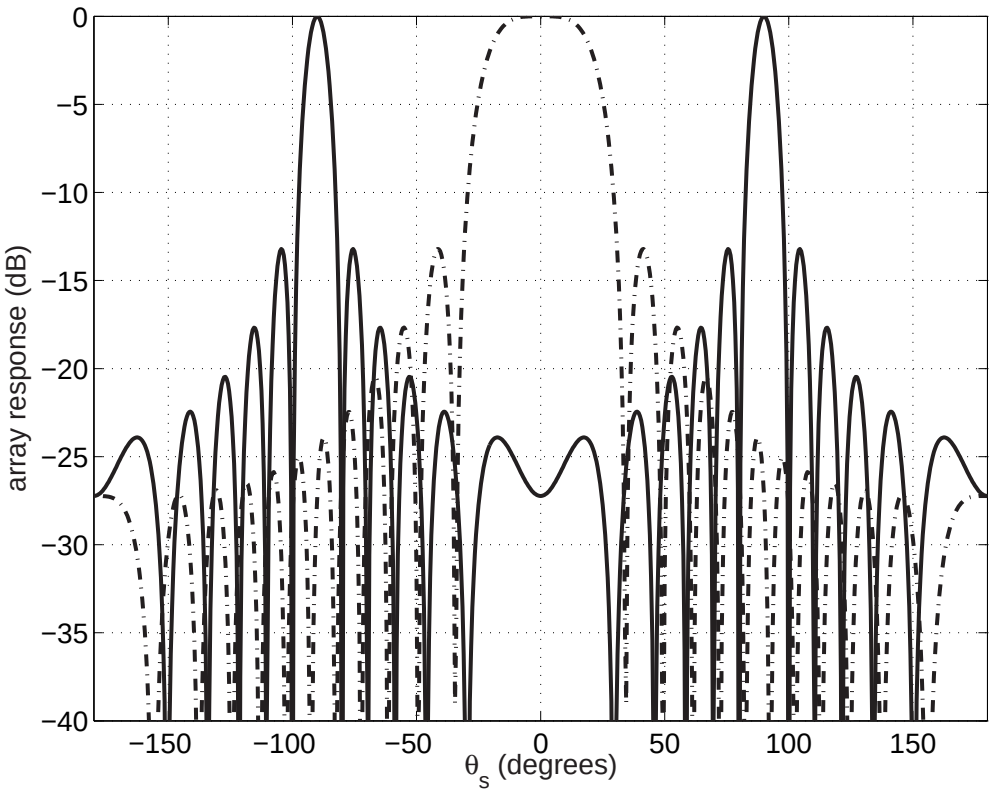

Figure 3-2: Array steered to (solid) broadside; (dashed) endfire

This type of beamformer is commonly referred to as a conventional beamformer. Different gains can be applied to each sensor output to change the beamwidth of the main lobe and sidelobe heights in the array beampattern.

3.1.2 The Ambient Noise Field

The ambient noise field of the ocean makes it difficult to accurately measure signal energy. Wenz [14] showed that ship traffic creates noise in the 50-500Hz range and can propagate more than 1000 miles. During World War II, measurements [15] of the deep-water noise field were taken in the 500Hz to 25kHz range. The results showed that breaking whitecaps, cavitation, wind-sea surface interaction, and surface waves all contributed to the ambient noise field. Other sources of noise include thermal, biological, engine noise, ocean turbulence, and seismic disturbances [1].

3.1.3 Adaptive Beamforming

With a weighting technique known as the Minimum Variance Distortionless Response beamformer (MVDR), or Capon beamformer, it is possible to minimize the variance of the beamformer output in the presence of noise. The ambient noise field must be accurately measured and the field must be stationary over the duration of the signal reception in order to obtain a good signal-to-noise ratio.

The two criteria for the MVDR beamformer are that it must minimize the variance of the output and it must be distortionless. MVDR beamformer weights are designed in the frequency domain. The beamformer is written as a sensor weight vector, $\mathbf{W}_o(\omega)$, where ω is radial frequency and the vector represents the weights applied to each sensor. Similar to the weighted least squares approach, the optimum weight vector can be determined by first deriving a distortionless constraint and then applying Lagrange multipliers. For more information on Capon beamformers, see Van Trees [12].

To start, the output of an array for a deterministic signal in the presence of noise is

$$\mathbf{X}(\omega) = \mathbf{X}_s(\omega) + \mathbf{N}(\omega), \tag{3.2}$$

where $\mathbf{X}_s(\omega)$ is the signal of interest and $\mathbf{N}(\omega)$ is the noise interference. The output of the beamformer is

$$Y(\omega) = \mathbf{W}_o^H(\omega)\left[\mathbf{X}_s(\omega) + \mathbf{N}(\omega)\right], \tag{3.3}$$

and, for a zero-mean random process, the expected value of the beamformer output is

$$E[Y(\omega)] = \mathbf{W}_o^H(\omega)\mathbf{X}_s(\omega). \tag{3.4}$$

For a plane wave signal arriving at angle θ_s this implies

$$\mathbf{W}_o^H(\omega)\mathbf{v}(\omega : \theta_s) = 1, \tag{3.5}$$

where $\mathbf{v}(\omega : \theta_s)$ is the output of the array. This is the distortionless constraint.

The variance of the output of the beamformer is

$$var[F(\omega)] = \mathbf{W}_o^H(\omega)\mathbf{S}_n(\omega)\mathbf{W}_o(\omega), \tag{3.6}$$

where $\mathbf{S}_n(\omega)$ is the spectral covariance matrix of the noise field. This value must be estimated and will be discussed later.

To impose the constraints we use a Lagrange multiplier and minimize

$$\begin{aligned} J \triangleq \mathbf{W}_o^H(\omega)\mathbf{S}_n(\omega)\mathbf{W}_o(\omega) + \lambda(\omega)\left[\mathbf{W}_o^H(\omega)\mathbf{v}(\omega : \theta_s) - 1\right] \\ +\lambda^*(\omega)\left[\mathbf{v}^H(\omega : \theta_s)\mathbf{W}_o(\omega) - 1\right]. \end{aligned} \tag{3.7}$$

Using complex gradients, and the distortionless constraint, the optimum weight vector is given by

$$\mathbf{W}_o^H(\omega) = \frac{\mathbf{v}^H(\omega : \theta_s)\mathbf{S}_n^{-1}(\omega)}{\mathbf{v}^H(\omega : \theta_s)\mathbf{S}_n^{-1}(\omega)\mathbf{v}(\omega : \theta_s)}. \tag{3.8}$$

Discrete-time broadband signal processing

The M-sequences generated by the two SPICEX sources were broadband signals with a 100Hz bandwidth, modulated to 250Hz. All of the array data were decimated to 781.25Hz to reduce processing time, which is above the Nyquist rate.

A Fast Fourier transform (FFT) must be applied to each sensor output. The FFT length must be chosen such that it is longer that the amount of time the signal takes to travel the length of the array at endfire. If L is the length of the array, and c is sound speed, κ is the lower FFT length limit given by

$$\kappa = \frac{L}{c}. \tag{3.9}$$

For data sampled at 781.25Hz, the lower limit on the FFT length is approximately 100. Baggeroer and Cox [16] suggested increasing the FFT lower limit to 8κ to avoid phase errors; this yields an FFT length limit of 794. The trade off of increasing

the FFT length is that it reduces the number of "snap-shots," frequency samples, available to estimate $\mathbf{S}_n^{-1}(\omega)$. I chose to use a 512-point FFT for all of the data files, which gives 1.53Hz frequency bins.

In MATLAB, the function *specgram* was used to efficiently transform the array data into the frequency domain, generating snap-shots of the frequency domain every 256^{th} sample. See Oppenheim [17] for more information on Fast-Fourier Transforms.

Spectral Noise Covariance Matrix Estimation

The SPICEX sources transmitted at predetermined times every hour. This made it possible to predict when a signal would arrive at the array given the location of the source and ship, and the speed of sound in the water. In effect, we had an active sonar system which allowed us to measure the spectral covariance matrix during time samples when the signal was not present. This matrix is used in the Capon algorithm, equation 3.8, to derive sensor weights.

An estimate of the spectral covariance matrix can be calculated using

$$\hat{\mathbf{S}}_n(\omega) = \frac{1}{K}\sum_{i=1}^{K}\mathbf{X}_i(\omega)\mathbf{X}_i^H(\omega), \tag{3.10}$$

where $\mathbf{X}_i$ is a vector of sensor outputs at snap-shot i. The most common criterion for choosing the number of snap-shots to estimate $\mathbf{S}_n(\omega)$ is to have $K > 2N$, as shown by Reed *et al* [18]. Carlson [19] suggested that diagonal loading can be used in the case where the number of snap-shots is between N and $2N$. Three reasons why fewer snap-shots might be used are: if there are not enough time samples to generate enough snap-shots, if the noise is not stationary, or if the array is physically turning.

In our experiment there was plenty of data immediately before and after each reception, allowing us to meet the criterion set by Reed. A low amount of diagonal loading was used because of very minor instability in the array during the experiment.

The diagonal loading for most of the data files was set to

$$d_{load} = \frac{1}{100} trace\left[\mathbf{X}_1(\omega)\mathbf{X}_1(\omega)^H\right]. \tag{3.11}$$

MVDR beamforming data

To process the data, I first estimated the spectral covariance matrix for each frequency bin using 361 snap-shots, only using frequency bins within the bandwidth of the M-sequence signals. I then calculated the optimum weight vector at each frequency bin for θ_s between 0° and 180°. These weight vectors were multiplied with the sensor data, in the frequency domain, for every snap-shot calculated from the recording, and the magnitude was plotted to determine arrival angle. Figure 3-4 is an example of the adaptive beamformer response showing time versus signal arrival angle. Using the beamformer response plot, the correct steering angle was determined for each signal. The time domain outputs for each sensor were then filtered using the beamformer frequency responses determined from the weights at each frequency bin at the desired angle. The *fftfilt* command in MATLAB was used to improve computation time. The filtered sensor outputs were then finally summed. The *fftfilt* function takes advantage of the overlap-add method of discrete time filtering; see Oppenheim [17] for more information on this method.

3.2 Matched Filtering

Matched filtering is a technique used to measure travel time, Doppler shift, and energy by correlating received signals with the transmitted signal. In the BASSEX experiment, M-sequence signals were used because their matched filter response is robust to noise. I used the power in the matched filter responses of each reception to measure the size of the perturbation zone behind the seamount.

For an arbitrary signal, $q(t)$, which passes through a waveguide with transfer

function $h(t)$, a single sensor output is given as

$$r(t) = q(t) * h(t). \tag{3.12}$$

The transfer function can be complicated in the ocean because attenuation and sound paths vary with frequency. In the 200-300Hz range, however, the attenuation and sound paths do not vary greatly; $h(t)$ can be simplified to a time delay and gain factor.

The matched filter implemented by convolving $r(t)$ with the original signal and the output is given by

$$y(t) = h(t) * q(t) * q(-t) = h(t) * R_q(t), \tag{3.13}$$

where $R_q(t)$ is the autocorrelation of the original signal. In the presence of noise signal $n(t)$, the output of the matched filter is

$$y(t) = h(t) * q(t) * q(-t) + n(t) * q(-t) = h(t) * R_{qq}(t) + R_{nq}(t). \tag{3.14}$$

The autocorrelation of any signal peaks at zero seconds. This property implies that the peak output of the matched filter will correspond to the time delay of the system and the size of the peak will indicate the attenuation.

For the purposes of my work, only relative signal strength is important. No effort was made to determine the amount of transmission loss, or attenuation, between the source and receiver and travel time is not determined; this is left for further study.

3.2.1 Measuring Doppler shift

The speed of the array relative to the sources creates a Doppler shift that must be applied to the reference signal before convolving it with data. The FORA array was towed between 3-4 knots throughout the experiment. The relationship between the

amount of Doppler shift and the receiver speed is [1]

$$f_D = \frac{f_c v}{c}, \tag{3.15}$$

where f_c is the frequency of the signal and v is the velocity of the receiver.

In order to get good matched filter performance it was necessary to estimate the Doppler shift before correlating the signals. A trial and error approach was used to estimate the Doppler shift. The original signal was stretched and compressed, then correlated with the beamformed array data. The correlation that gave the highest response was taken as the final matched filter output. Energy calculations for each reception were made by summing the square of the absolute value of the matched filter output.

Each M-sequence signal transmitted by the SPICEX sources contained 12 periods. Small variability in the speed of the ship, due to environmental factors, compelled us to sample the Doppler shift during each period of every reception. This resulted in a stronger matched filter output.

Matched Filter Results

Figures 3-3 through 3-8 show example matched filter results from data file *jd264142234-KauaiSpice.DAT*. Figure 3-3 is a chart showing the location where the signal reception was made. The black line connects the array and source S1 and the red line connects the array and source S2.

Figure 3-4 is the beamformer response during the recording of the two SPICEX sources. The sound from S2 is known to arrive first given its distance to the array compared with S1. This and the figure imply that the signal from S1 is arriving at approximately 20 degrees off endfire and the signal from S2 is arriving at approximately 50 degrees off endfire.

Figures 3-5 and 3-7 show the Doppler shift versus period which needs to be applied to the reference signal used in the matched filter. This figure was generated

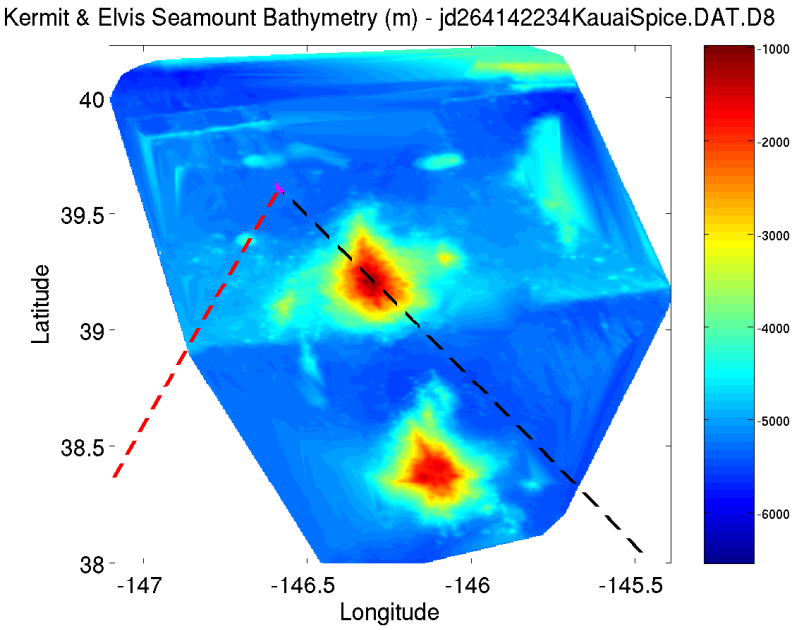

Figure 3-3: Data file jd264142234KauaiSpice.DAT.D8

by dividing the received signal into 50% overlapping sections, each two M-sequence periods long, and matched filtering them with a reference signal. The reference signal was stretched and compressed to mimic Doppler shifts. A range of Doppler shifts were tried and the results were compared to find a maximum; this is an estimate of the correct Doppler shift for each period. In both of these cases the array's speed and direction were constant and the Doppler shift did not change versus time.

Figures 3-6 and 3-8 show the matched filer results for each signal. Again, the received signal is divided into two-period-long segments with 50% overlap. The reference signal, with the correct Doppler shift, was convolved with each segment. The received signal was divided into segments to view changing Doppler shift and estimate arrival time. The figures show multiple arrivals for both M-sequence signals as near-vertical lines with slopes related to the speed and angle of the array relative to the source.

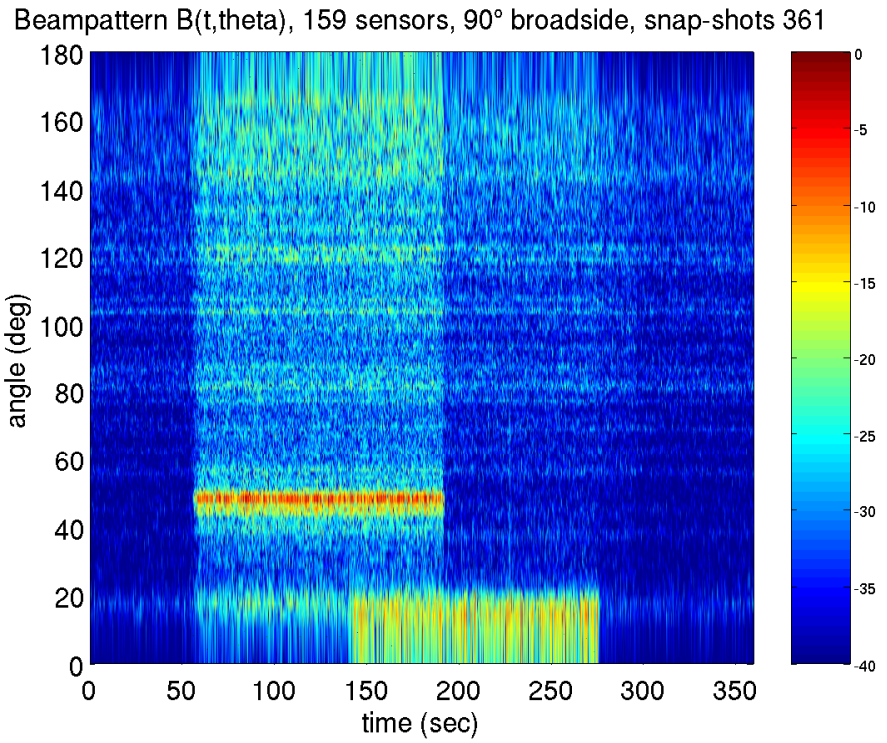

Figure 3-4: Data file jd264142234KauaiSpice.DAT.D8

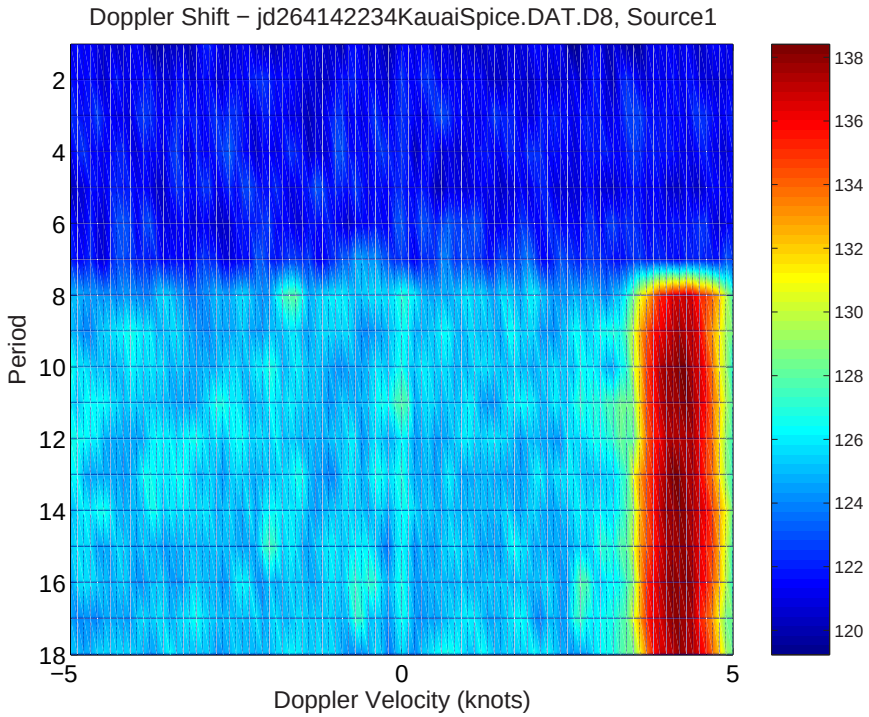

Figure 3-5: Data file jd264142234KauaiSpice.DAT.D8

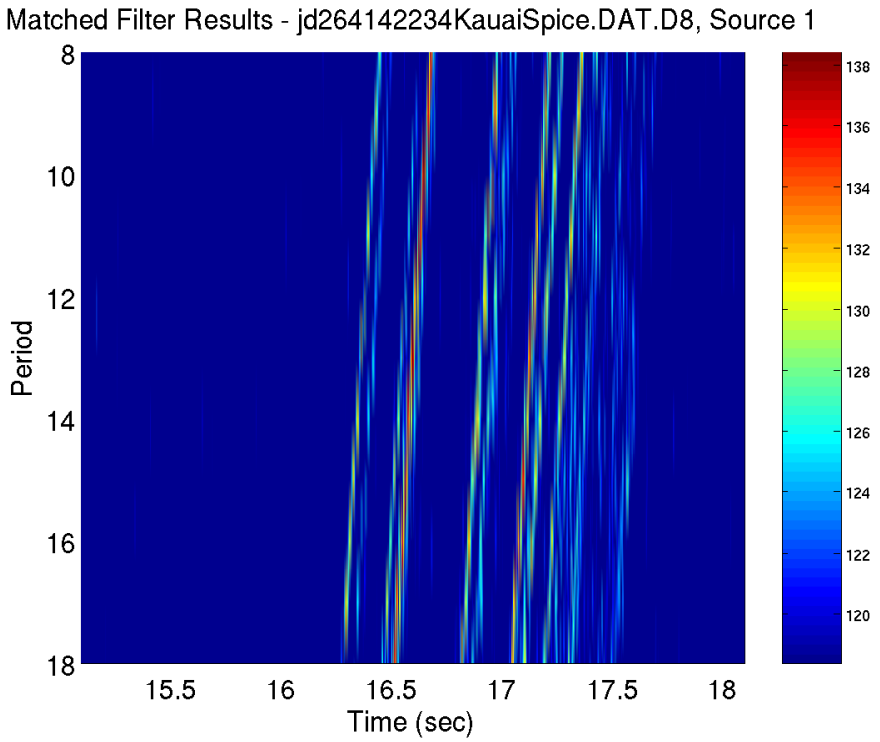

Figure 3-6: Data file jd264142234KauaiSpice.DAT.D8

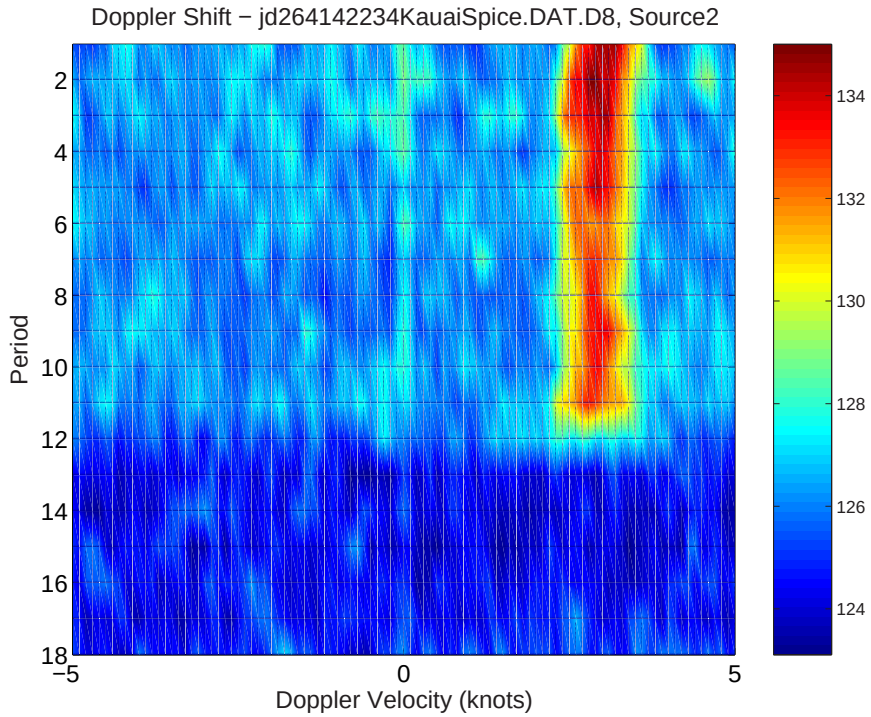

Figure 3-7: Data file jd264142234KauaiSpice.DAT.D8

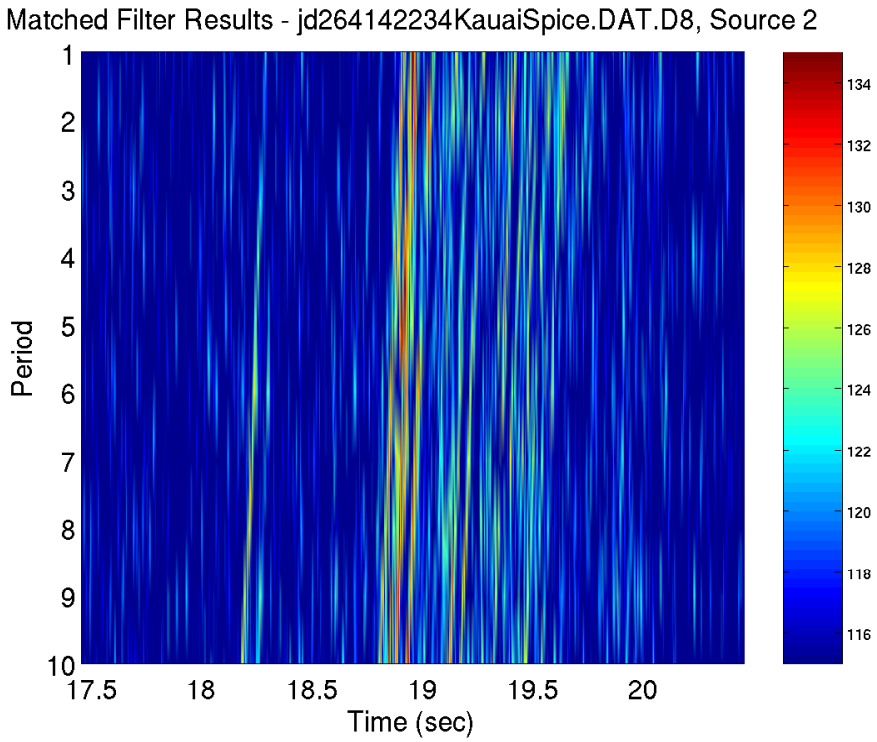

Figure 3-8: Data file jd264142234KauaiSpice.DAT.D8

3.2.2 LOAPEX recording glitches

Period-by-period matched filtering revealed "glitches" in the LOAPEX recordings. Occasionally, pieces of data would simply be lost. They usually occurred approximately 300 seconds into each recording. These glitches effectively shrunk the received signal, making it appear to have gone through a dramatic Doppler shift of over 20 knots, rather than the expected 0-4 knots.

For most recordings, there were few to no glitches in the SPICEX reception recordings.

Chapter 4

Results

The perturbation zone behind the Kermit-Roosevelt Seamount was measured by beamforming and matched-filtering signal receptions recorded in that region. I predicted that a shadow zone would form behind the seamount, containing regions of high and low acoustic energy, between 10 and 15dB, and that it would heal itself far behind the seamount.

4.1 Adaptive Beamforming Results

I used an MVDR beamformer to process the data from the cruise for an improved signal-to-noise ratio. This is especially needed at array endfire: the array's resolution was poorest at endfire, noise from the ship engine arrived at endfire, and it was common to have M-sequence signals arrive at endfire. There were more than enough data before and after each signal reception to accurately measure the spectral covariance matrix. For every reception, the diagonal loading was set to 0.01, and 361 snap-shots were used to estimate the spectral covariance matrix. Refer to Appendices C-F to see the output from the beamformer and matched filter for each signal reception.

4.1.1 SPICEX Source 1 (S1)

Figure 4-1 shows the acoustic energy measured from S1 around the Kermit-Roosevelt Seamount Complex. Each dot represents a location where we processed an M-sequence. The solid, maroon contour lines are on the two tallest seamounts in the complex, providing a reference. The arrow indicates the arrival direction of the signal from source S1. A cubic interpolation algorithm was used in MATLAB to fill in regions of the chart where processed data was not available. Some kriging can be observed in regions were data is unavailable.

A region of lower acoustic energy directly behind the northern-most seamount is shown in the figure. This region has areas of relatively lower and higher acoustic energy, going away from the seamount. From the data available, it is not possible to state conclusively that the perturbation zone heals itself far behind the seamount; however, it appears to heal to some degree. This is due to a lack of data in areas outside of the perturbation zone.

4.1.2 SPICEX Source 2 (S2)

Figure 4-2 shows the acoustic energy measured from S2 around the Kermit-Roosevelt Seamount Complex. Sound from S2 is arriving from the left corner. This chart clearly shows a perturbation zone behind both the northern and southern seamounts. The shadow zone behind the upper seamount appears to be stronger, perhaps since it is the larger of the two seamounts. Again, there are not enough data behind the northern-most seamount to conclusively say that the perturbation zone heals itself, however, the southern-most seamount has more data behind it and there is a good indication that the zone decreases in size and intensity far from the seamount.

This figure strongly supports my predictions about the shape of the perturbation zone. There are data points in this example that run perpendicular to the sound path between S2 and the northern-most seamount. These data points show that the perturbation zone does indeed fan out behind the seamount.

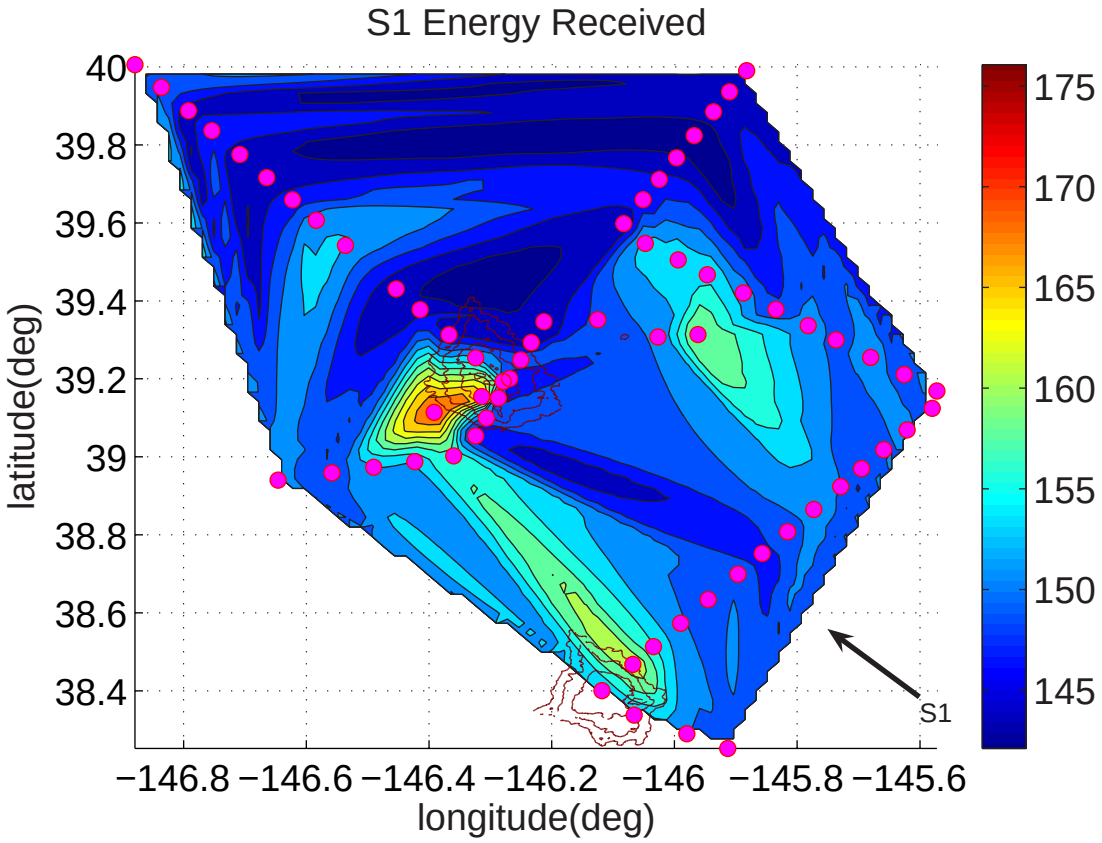

Figure 4-1: Received SPICEX Source 1 acoustic energy (dB)

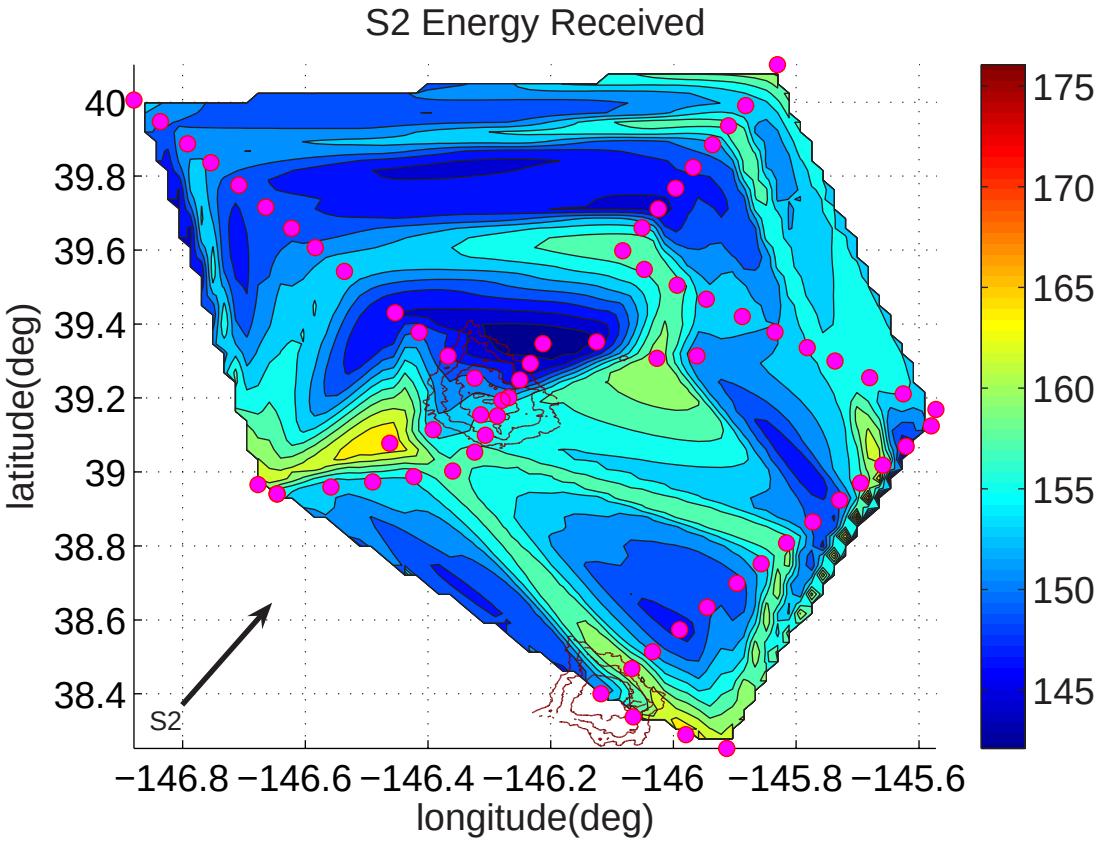

Figure 4-2: Received SPICEX Source 2 acoustic energy (dB)

4.2 Summary

The perturbation zone

The figures indicate that a perturbation zone formed behind each of the seamounts. The scattering field was more visible in the S2 results. The shape of this perturbation zone was consistent with theory; it fanned out behind the seamount and appeared to heal itself.

Values in the perturbation zone

The acoustic energy inside of the shadow zone varied, with higher and lower regions, compared with the surrounding field. The levels stayed within about 10dB inside of the perturbation zone.

Adaptive beamforming method

The adaptive beamforming method reduced endfire noise and separated M-sequence receptions well. Some data files could not be processed, however, because of high noise levels, unexpected array movement, or missing signal receptions. Figures showing beamformer response, matched filter output, doppler shift, and ship location for each of the recordings processed are included in the appendices.

Chapter 5

Conclusion

5.1 Summary

In this thesis I explored how seamounts scatter acoustic energy through experimentation and signal processing methods. I used a towed hydrophone array to listen to distant underwater sources in the Pacific Ocean in order to accurately measure the size of the perturbation zone behind the Kermit-Roosevelt Seamount.

By analyzing receptions from the two SPICEX sources, it was possible to visualize the perturbation zone behind the seamount. The size and shape of the perturbation zone was consistent with the theoretical model. Numerous signal receptions were obtained in straight lines directly behind the seamounts.

Three improvements which could have been made to our experiment are:

- the addition of more side-to-side ship tracks to get an accurate measure of the width of the perturbation zone.
- the extension of the ship track further behind the seamount to determine the distance needed to heal the perturbation zone.
- the addition of parallel ship tracks outside of the perturbation zone to give a clear reference energy level.

5.2 Future Work

There are many ways to extend this research. While this thesis focused entirely on experimental results, numerical simulation could be used to further our understanding of the effect of seamounts on sound propagation. Two specific ways in which this research could be continued, beyond the improvements stated earlier, are:

- *Experimentation.* Use data from the NPAL experiment to identify different sound paths to better understand the scatter field, in particular the diffraction extent of the seamount. Different types of adaptive beamformers should be explored to improve array resolution, especially at endfire, in the 0-250Hz frequency range.

- *Use of computational acoustic modelers to validate results.* Normal mode or parabolic acoustic modelers could be used to predict the scattering field around the Kermit-Roosevelt Seamount; discussed in Jensen *et al* [20]. Two codes I recommend are C-SNAP, produced by SACLANTCEN, and Range-dependent Acoustic Modeler (RAM), a program written by Dr. Michael Collins for ONR. C-SNAP is an accurate coupled-mode acoustic modeler and RAM is an fast parabolic approximation acoustic modeler, primarily used by the U.S. Navy. To model the scatter field around a seamount, a three dimensional acoustic modeler will most likely be needed.

Appendix A

Nomenclature

boldface variables represent column vectors or matrices

c	=	sound speed
T	=	temperature
S	=	salinity
z	=	depth
m	=	meters
s	=	seconds
Hz	=	hertz
kHz	=	kilohertz
dB	=	decebel
τ_n	=	time delay for sensor n
p	=	distance of sensor n from reference sensor
H	=	Hermetian transpose (complex-conjugate transpose)
ω	=	radians per second
$\mathbf{x}^*$	=	complex conjugate of $\mathbf{x}$
N	=	number of array sensors

θ_s	=	steering direction
$\mathbf{S}_n(\omega)$	=	spectral covariance matrix
$\hat{\mathbf{S}}_n(\omega)$	=	estimate of the spectral covariance matrix
$R_q(t)$	=	autocorrelation of q(t)
$R_{nq}(t)$	=	cross-correlation of n(t) and q(t)
$\mathbf{W}_o(\omega)$	=	MVDR weigth vector
$\mathbf{v}(\omega : \theta_s)$	=	array output for plane wave arriving at θ_s
$\lambda(\omega)$	=	Lagrange multiplier at frequency ω
$*$	=	convolution

Appendix B

Computing technical detail

The computations described in this thesis were performed using IBM-PC compatible computers running the Redhat Linux operating system. Linux is a free OS for computers using the Intel and Alpha microprocessors. More information on Linux can be obtained from http://www.linux.org.

My code was written entirely in Matlab. This is a high-level computer environment for numerical computation and visualization marketed by The MathWorks (http://www.mathworks.com). The signal processing toolbox was used to perform fast Fourier transforms, filtering, and data visualization.

Purchased for the BASSEX experiment, a computer containing a 3.2GHz CPU, 2GB of RAM, and 1TB of hard disk space was used to run my Matlab code. A second identical machine was purchased as part of the experiment for data storage. Raw data was stored on 250GB SATA hard drives.

Bibliography

[1] R.J. Urick. *Sound Propagation in the Sea.* (Defense Advanced Research Projects Agency, Washington D.C., 1979).

[2] Kathleen E. Wage. *Broadband Modal Coherence and Beamforming at Megameter Ranges.* PhD thesis, Massachusetts Institute of Technology, 2000.

[3] Gordon R. Ebbeson and R. Glenn Turner. Sound propagation over Dickins Seamount in the Northeast Pacific Ocean. *J. Acoust. Soc. Am.*, 73:143–152, 1983.

[4] M.I. Taroukadis. A coupled-mode formulation for the solution of the helmholtz equation in water in the presence of a conical seamount. *Journal of Computational Acoustics*, 4:101–121, 1996.

[5] Jérémie Eskenazi. A computer model for sound propagation around conical seamounts. Master's thesis, Massachusetts Institute of Technology, 2001.

[6] Clarence S. Clay and Herman Medwin. *Acoustical Oceanography: Principles and Applications.* John Wiley & Sons, Inc. New York, 1977.

[7] Xavier Lurton. *An Introduction to Underwater Acoustics.* Praxs Publishing, Chichester, UK, 2002.

[8] James Mercer, Rex Andrew, Bruce Howe, and John Colosi. Cruise Report: Long-range Ocean Propagation Experiment. Technical report, Applied Physics Laboratory, University of Washington, Woods Hole Oceanographic Institute, 2005.

[9] W.H.F. Smith and D.T. Sandwell. Global Sea Floor Topography from Satellite Altimetry. *Science*, 277(5334):1956–1962, 1997.

[10] GEBCO Bathymetric Grid. <http://www.ngdc.noaa.gov/mgg/gebco/grid/1mingrid.html>, Mar 2004.

[11] H. Medwin. *Fundamentals of Acoustical Oceanography.* Academic Press, Sandiego, 1997.

[12] Harry L. Van Trees. *Optimum Array Processing*, volume IV of *Detection, Estimation, and Modulation Theory.* John Wiley & Sons, Inc., New York, 2002.

[13] B. Hofmann-Wellenhof, H. Lichtenegger, and J. Collins. *GPS Theory and Practice.* New York: Springer-Verlag, Wein, 1992.

[14] G.M. Wenz. Acoustic Ambient Noise in the Ocean: Spectra and Sources. *J. Acoust. Soc. Am.*, 34:1936, 1962.

[15] V.O. Knudsen, R.S. Alford, and J.W. Emling. Underwater ambient noise. *J. Mar. Res.*, 7:410, 1948.

[16] A. Baggeroer and H. Cox. Passive sonar limits upon nulling multiple moving ships with large aperture arrays. *Proceedings of the 33rd Aslomar Conference on Signals, Systems & Computers (Pacific Grove, CA)*, pages 103–108, Nov. 1999.

[17] A.V. Oppenheim and R.W. Schafer. *Discrete-Time Signal Processing.* Prentice-Hall, 1989.

[18] I.S. Reed, J.D. Mallat, and L.E. Brennan. Rapid convergence rate in adaptive arrays. *IEEE Trans. Aerosp. Electron. Syst.*, AES-10:853–863, Nov 1974.

[19] B.D. Carlson. Covariance matrix estimation errors and diagonal loading in adaptive arrays. *IEEE Trans. Aerosp. Electron. Syst.*, 24:397–401, July 1988.

[20] Finn B. Jensen, William A. Kuperman, Michael B. Porter, and Henrik Schmidt. *Computational Ocean Acoustics.* Springer-Verlag New York, Inc., 2000.